Chemistry–A European Journal
Research Article
doi.org/10.1002/chem.202300987
Chemistry Europe
European Chemical Societies Publishing
www.chemeurj.org

Controlling Swing Rates in Macrocyclic Molecular Mortise Hinges

Alexander J. Menke,[a] Joseph M. Mellberg,[a] Hongjun Pan,[b] Joseph H. Reibenspies,[c] Benjamin G. Janesko,*[a] and Eric E. Simanek*[a]

Abstract: Hinge motion is observed in macrocyclic, mortise-type molecular hinges using variable temperature NMR spectroscopy. The data is consistent with dynamic hinging from a folded-to-extended-to-folded enantiomeric state. Crystallographic and solution structures of the folded states are reported. Chemical shift predictions derived from crystallographic data corroborate fully revolute hinge motion. The rate of hinging is affected by steric congestion at the hinge axis. A macrocycle containing glycine, **1**, hinges faster than one comprising aminoisobutyric acid, **2**. The free energies of activation, $\Delta G^{\ddagger}$, for **1** and **2** were determined to be 13.3 ± 0.3 kcal/mol and 16.3 ± 0.3 kcal/mol, respectively. This barrier is largely independent of solvent across those surveyed (CD_3OD, CD_3CN, DMSO-d_6, pyridine-d_5, D_2O). Experiment and computation predict energy barriers that are consistent with disruption of an intramolecular network of hydrogen bonds. DFT calculations reveal a pathway for hinge motion.

Introduction

Hinges are pervasive. At the molecular level, Nature employs hinge domains to facilitate motion with noteworthy examples including immunoglobins[1] and proteins engaged in DNA-binding[2] and motility.[3] In the nanoworld, hinges join tweezers,[4] switches,[5–8] motors,[9–13] valves,[14] shuttles,[15,16] gears,[17] and pumps[18,19] in the toolbox of molecular machinists.

In the macroscopic world, mortise hinges open doors. They comprise two leaves that stack against each other in a co-planar fashion. Holes in the leaves facilitate their attachment to objects of interest vis-à-vis a door and frame such that the surfaces of the hinge and the objects to which it is attached are flush. Standing alone, mortise hinges typically display a 360° range of motion – the leaves sweep a full circle allowing both faces to have the opportunity for intimate contact.

Molecular hinges need not rely on a pin and knuckles like their macroscopic namesakes. Instead, leaves typically move by rotations about a single bond in linear molecules or through the coordinated contortions of macrocycles. Indeed, macrocycles are counted amongst the earliest identified "molecular hinges." Gutsche described calix-[6]-arenes as "hinged" if three consecutive arenes were disposed upward and the subsequent three adopted the opposite orientation.[20] To the best of our knowledge, Hamilton coined the term to describe the 34° swinging motion executed by a naphthalene group to engage in π–π stacking following a recognition event by an artificial receptor.[21,22] The designation "molecular hinge" has been applied to isosteres of proline,[23] a small molecule host that scissors upon binding a guest,[24] flexible, azacyclohexane domains of a rigid, norbornene scaffold,[25] and conformational switching resulting from single-bond rotations in pyridines and bipyridines.[26,27] The incorporation diazo groups into a macrocyclic backbone has led to a photoswitchable macrocyclic hinge.[28] Hinges have been controlled with pH[29] and redox chemistry.[30]

While describing a poly(aromatic), 20-atom macrocycle, Slater and coworkers articulated additional, desirable properties of a molecular hinge.[31] These elements include favorable solubility, facile synthesis, well-defined open and closed states, and chemical inertness vis-à-vis an inability to engage in recognition events. This final criterion effectively distinguishes hinges from tweezers. Applying these definitions, the number of molecular hinges reported in the literature is limited.

Now, additional care is being taken to better describe the nature of the hinge produced. For example, pivot hinges have been described by Zhao and coworkers in the creation of metal–organic frameworks (Scheme 1).[32] In addition to the characteristics advanced, we further differentiate mortise hinges from other hinge structures by virtue of their 360° range of

[a] A. J. Menke, J. M. Mellberg, Dr. B. G. Janesko, Dr. E. E. Simanek
Department of Chemistry & Biochemistry
Texas Christian University
Fort Worth, TX 76129 (USA)
E-mail: b.janesko@tcu.edu
e.simanek@tcu.edu

[b] Dr. H. Pan
Department of Chemistry
University of North Texas
Denton, TX 76203 (USA)

[c] Dr. J. H. Reibenspies
Department of Chemistry
Texas A&M University
College Station, TX 77845 (USA)

Supporting information for this article is available on the WWW under https://doi.org/10.1002/chem.202300987

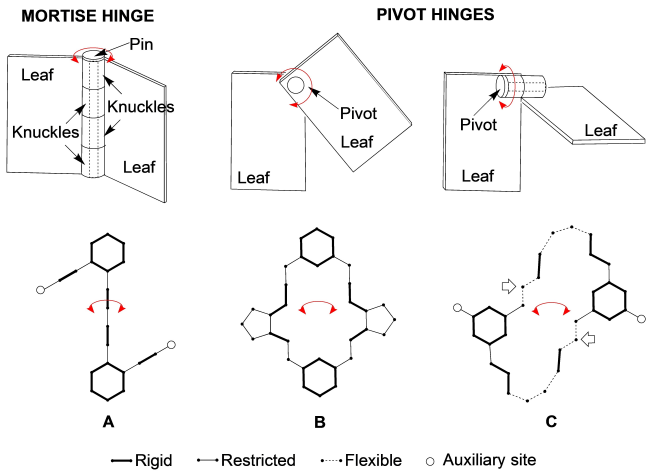

Scheme 1. Mortise and pivot hinges. Annotated Murcko frameworks of molecular hinges appear beneath the macroscopic, labelled hinges. The shaded areas convey leaf and pin elements. The red arrow shows hinge motion. On **C**, the arrows indicate the sites of substitution that differentiate the hinges described here.

motion such that coplanar stacking (eg. π–π) of the leaves is facilitated.

Scheme 1 introduces annotated Murcko frameworks of three hinges, **A**–**C**.[33] The open circles identify sites for attachment of other groups to the leaves. The weight of the line reports on flexibility. Dark lines correspond to rigid sp^2–sp^2 bonds including aromatic rings and amide bonds. Unweighted lines correspond to restricted rotors. Dashed lines denote less restricted sp^3–sp^3 bonds. Effort is made to be true to – or at minimum, to effectively communicate – bond angles.

Sankararaman's hinge, **A**, represents the earliest mortise-like hinge reported, although it was not expressly identified as such. The rigid dialkyne backbone connotes a macroscopic hinge's pin.[34] While the leaves may not be wholly flush, they sweep much of the accessible 360° arc and afford π-stacking of the pendant terephenylene groups (circles). An earlier study incorporated pyrene groups into a hinge limited to 180° rotation.[35] Hinge **A** was recently adopted to explore solvent-mediated conformational changes to phosphoresence when organometallic chromophores were attached to the leaves.[36] Slater's hinge – a macrocycle represented by **B** – allows the leaves to stack by transitions from open to closed states in solution.

Here, we describe macrocycles that employ framework **C**. This scaffold allows 360° movement of leaves and the co-planar stacking of π-systems. Unique amongst the mortise-like hinges described, this framework incorporates flexible domains, and in doing so, offers the opportunity to manipulate dynamic motion. These hinges derive from 24-atom macrocycles that differ in the choice of amino acid. Moving from glycine to aminoisobutyric acid – from CH_2 to $C(CH_3)_2$ – preserves hinge characteristics, but reduces the rate of hinge motion. The site of this substitution is indicated with arrows on the annotated Murcko frameworks.

Results and Discussion

Synthesis and nomenclature

Assembling molecular hinges **1** and **2** from monomers – like those of the macroscopic world – is quantitative and attributed to intermediates pre-organized by networks of hydrogen bonds.[37] That is, **1** and **2** are the sole products of the acid-catalyzed dimerization of α,ω-monomers containing an acetal and protected hydrazine group (Scheme 2).[37–40] The synthesis and characterization of **1** has been described.[38] The preparation of **2** follows the same route.[38]

Briefly, the monomers are obtained in two steps starting with the one-pot, sequential substitution of trichlorotriazine to yield the carboxylic acid intermediate. Substitution commences with additions of BOC-hydrazine, followed by the amino acid of interest and a third auxiliary amine. This final addition to these triazine leaves, metaphorically, is the door and frame. Here, either morpholine or dimethylamine groups are incorporated and the results are molecules that are flush like their macroscopic namesake. Morpholine groups promote crystallization while dimethylamine groups simplify the NMR spectrum. The second step in the sequence yields monomer by amidation with the amino acetal.

Crystallographic analysis

Both **1** and **2** yielded crystals suitable for x-ray analysis. The single structure obtained for each shows both **1** and **2** in the closed state (Figure 1). The leaves – the extended π-network derived from the triazine and hydrazone – stack upon each other in an arrangement that is descriptively coplanar. Deviations from coplanarity in hinge **2** are attributed to crystal packing forces. Critically, the crystal structures reveal that hydrogen atoms on carbons B, C, α (of **1**) as well as the β-methyl groups (of **2**) occupy different chemical environments which we distinguish with the labels (a)xial and (e)quatorial.

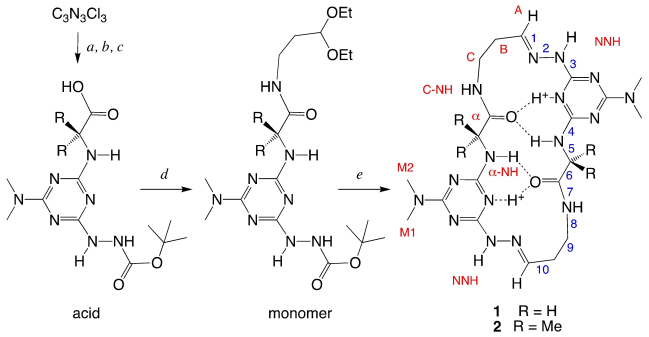

Scheme 2. Synthesis of the macrocycles. a) BOC-hydrazine, 0 °C, NaOH*(aq)*; b) amino acid, RT to 50 °C; c) CH_3NHCH_3; d) 3-amino-1,1-diethoxypropane, HBTU, HOBT, RT; e) 1 : 1 TFA : CH_2Cl_2. NMR labels are shown in red. Rotors are numbered in blue.

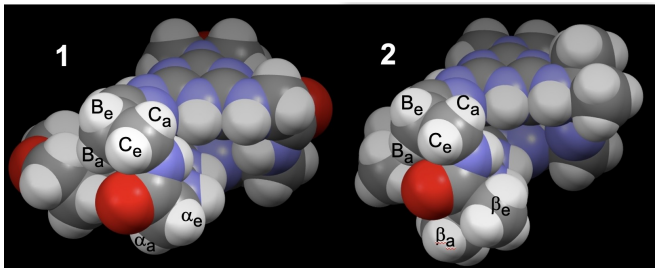

Figure 1. The solid-state structures of hinges **1** and **2** with solvent excluded for clarity. Protons on methylenes B, C and α and the β-methyl groups are identified with the subscripts (a)xial or (e)quatorial.

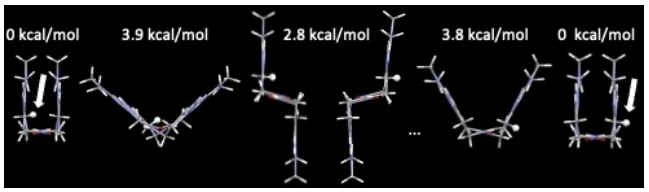

Figure 2. DFT calculations of hinge motion showing relative energies in kcal/mol) for each conformation. One hydrogen atom of B is indicated with an arrow to show interconversion.

Solution state geometries

Solution ^{1}H NMR studies provide additional evidence for the closed geometries for **1** and **2**, confirming that the solid state and solution structures of the closed hinge are very similar. Common features include *(E)*-hydrazones (dihedrals 1 and 2; Scheme 2), protonation opposite the auxiliary dimethylamine group, adoption the same rotamer state resulting from hindered rotation about the triazine-N bonds (dihedrals 3 and 4),[42,43] and an rOe between "A" and "M1" that is only rationalized by folding. A model for assessing solution structure based on chemical shifts and rOe connectivities has been described and additional details appear in the Supporting Information.[40]

One structural element differs significantly in the solution and solid-state structures of **1** and **2** – the orientation of the amide. In the solid state, the amide carbonyls are oriented outward (C═O out) to bridge unit cells as shown in Figure 1. In solution, the amide carbonyls are oriented inward (C═O in) to participate in a network of stabilizing hydrogen bonding interactions. The "C═O in" orientation has been observed in the solid-state structures of macrocycles incorporating valine and isoleucine. The conformational freedom surrounding the amide – dihedrals 6 and 8 – is noteworthy in that it offers insights into the mechanistic basis for hinge motion.

Modeling hinge motion with DFT calculations

DFT calculations were performed to develop a model of hinge motion. Figure 2 shows different states of **1** on the free energy surface. The relative energies are indicated in kcal/mol. We hypothesize that hinge motion – from closed to open to closed – proceeds much like its macroscopic analogue. In the early stage, rotations about the free rotors (dihedrals 5 (Φ), 6 (Ψ), 8, 9, 10) open the hinge. These movements are identical for both subunits until the hinge opens to more than 90° at which time, disrotary rotations about Φ and Ψ lead to a partially extended state. Passing through to a pseudo-planar (flat) transition (not shown), the enantiomeric, extended state is reached followed by collapse back to the closed hinge with resumption of conrotary rotations. Throughout these machinations, the network of hydrogen bonds is largely preserved, although the orientations (and presumably energetics) of these interactions change.

Observing hinge motion using NMR spectroscopy

Evidence for hinge motion comes from variable temperature ^{1}H NMR spectroscopy. The ^{1}H and ^{13}C NMR spectra for **1** and **2** are markedly similar. The fingerprint region of the ^{1}H NMR between 7–13 ppm shows evidence for the hydrazone, hydrogens labeled 'A', as well as exchangeable protons NNH, H^+, α–NH and C–NH. This region does not change with temperature except for modest temperature-dependent migrations of the resonances. However, features in the upfield region of the spectrum change dramatically with temperature. Coalescence of resonances corresponding to the α-hydrogens of **1**, β-methyl groups of **2**, as well as hydrogens on B and C all reveal the swinging of the hinge.

Figure 3 shows the variable temperature spectra for **2**. At room temperature in CD_3OD, the hydrogens labeled C and B (blue and green, respectively) are distinct and the methyl groups (red) have begun to coalesce. As the temperature is increased, coalescence is observed for all three sets of resonances. Similar behavior is observed for **1** at lower temperatures.[38]

DFT predictions of chemical shifts support hinge motion

The predicted ^{1}H chemical shifts link solid-state and solution structures, and support the hypothesis that the observed chemical shifts arise from full 360° interconversion. Minimizing the solid state structures of **1** and **2** yielded the "C═O in" geometry. Table 1 shows the predicted and experimental chemical shifts. Calculations on **1** predict that the resonances at 4.46 ppm and 3.03 ppm arise from the axial and equatorial hydrogens C. The resonance observed at 2.64 ppm arises from the coalescence of the axial and equatorial hydrogens B. Resonances observed at 4.17 and 3.89 correspond to α. Calculations on **1** show that a full 360° rotation interconverts these pairs of hydrogens, consistent with the observed coalescence of these resonances (Figure 4). Figure 2 traces the interconversion of one of the hydrogen atoms on B (shown with arrow).

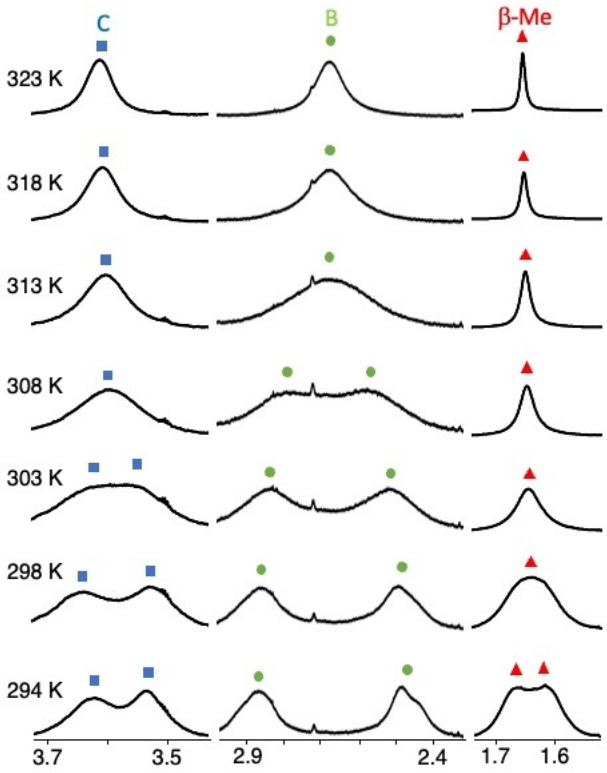

Figure 3. Portions of the 400 MHz NMR spectra of **2** in CD_3OD. Hydrogens corresponding to C (blue), B (green) and the geminal dimethyls (red) are indicated.

Similar conclusions hold for **2**. In particular, the two resonances at 2.89 ppm and 2.41 ppm arise from the axial and equatorial hydrogens B, while those at 1.67 ppm and 1.58 ppm arise from the two β-methyl groups. These calculated values are largely independent of solvent surveyed. Here, methanol is used as the computational and experimental solvent.

Coalescence temperatures, exchange rates and $\Delta G^{\ddagger}$

Coalescence temperatures (T_c), exchange rates (k_{exch}) and $\Delta G^{\ddagger}$ can be determined. Coalescence temperatures can be calculated by plotting chemical shift as a function of temperature, and subsequently identifying the intersection point of the lines fit to the data. The margins of error derive from ambiguities associated with the line fits for each assignment. These errors are shown as shaded triangles. For consistency, the center of this region was chosen as T_c and an error estimate corresponding to ±2.5 K was assumed. Even with this liberal error range, the impact on $\Delta G^{\ddagger}$ is insignificant (±0.1 kcal/mol).

From these data, rate constants (k_{exch}) at the coalescence temperature were determined using Equation (1) where Δν is the difference in chemical shifts of the resonances when fully decoalesced. Table 2 summarizes the results of these calculations.

$$k_{exch} = \pi(\Delta\nu)/\sqrt{2} = 2.22(\Delta\nu) \quad (1)$$

Using the Eyring equation (Eq. (2)) the free energy of activation, $\Delta G^{\ddagger}$, can be calculated. Here, κ, the transmission coefficient, is assumed to be 1, h is the Planck constant, k_B is the Boltzmann constant, R is the gas constant and T_c is the coalescence temperature.[43]

$$\Delta G^{\ddagger} = -\ln((\kappa h k_{exch})/(k_B T_c)) * RT_c \quad (2)$$

A common $\Delta\Delta G^{\ddagger}$ is consistent with a process independent of solvent. The results shown in Table 2 reveal good agreement for $\Delta G^{\ddagger}$ across the resonances for a given macrocycle. On average, $\Delta G^{\ddagger}$ is 13.3±0.3 kcal/mmol for **1**, and 16.3±0.3 kcal/mol for **2**. These values are in line with the cost of breaking the hydrogen bond network, calculated to be 14 kcal/mol.[37] Models show that the geometries of these interactions are affected and the network may disappear transiently in the flat, extended intermediate. At the current level of theory and model systems, the qualitative picture that emerges is one in which these modestly flexible. macrocycles can orchestrate motions to minimize energetic penalties associated with breaking hydrogen bonds and adopting unfavorable torsions. The 3 kcal/mol difference is attributed to steric congestion at the site of hinge motion, notably dihedral 5.

Energetic costs for rotamer interconversion

In *neutral* systems, the barrier for rotation about the triazine-N bond has been measured to be as low as 13 kcal/mol[42] and calculated to be as high as 22 kcal/mol.[43] This barrier is likely higher for the protonated triazines described here. Using the dimethylamine group as a reporter of rotamer interconversion, its appearance as two well-resolved singlets across much of the temperature range suggests that rotation about triazine-N bonds is not involved in hinge motion.

To obtain a better estimate of this barrier, **2** was heated in pyridine-d_5. Coalescence of methyls M1 and M2 is observed at 75 °C, corresponding to a $\Delta G^{\ddagger}$ = 18.0 kcal/mol. We currently

Table 1. Predicted (Calc) and observed chemical shifts (at the indicated temperature in K) in the ^{1}H NMR reported in ppm.

	B_e	B_a	C_a	C_e	β_a	β_e	α_a	α_e
1-Calc	2.82	2.57[a]	4.43	3.01	–	–	4.12	3.82
1-226	2.63	–[a]	4.46	3.03	–	–	4.17	3.89
2-Calc	2.90	2.59	4.48	3.04	1.85	1.65	–	–
2-256	2.89	2.41	3.63	3.51	1.67	1.58	–	–

[a] Decoalescence was not observed. The coalesced value is reported.

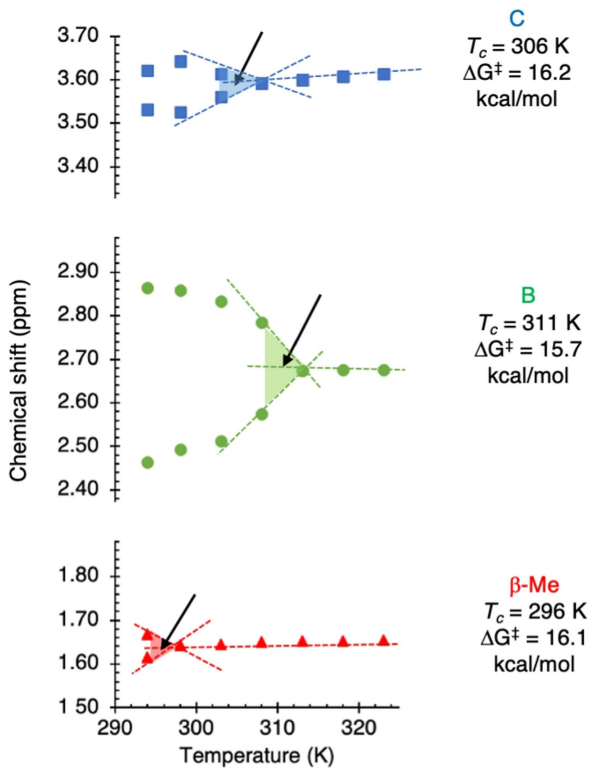

Figure 4. Plots of chemical shift versus temperature are used to calculate Tc.

posit that the energy difference between this value and that observed for hinge motion in **1** (13.3 kcal/mol; Δ = 4.5 kcal/mol) is sufficient to abandon this possibility that rotamer interconversion contributes to hinge motion. While the difference is much smaller for **2** (Δ = 1.4 kcal/mol), we favor a model wherein **2** hinges like **1** because methyls M1 and M2 do not coalesce during these experiments, either.

Experimental Section

General chemistry and synthesis

Details of the synthesis, purification, and characterization of macrocycles and their precursors appears in the Supporting Information.

NMR spectroscopy

All 1D ^{1}H NMR and ^{13}C{1H} NMR spectra occurring at room temperature and higher were recorded on a 400 MHz Bruker Avance spectrometer at Texas Christian University. Chemical shifts were referenced to the corresponding solvent resonances. Low temperature spectra were acquired on a 500 MHz Varian NMR spectrometer at the University of North Texas in Denton. All structural assignments were made utilizing information from COSY and HSQC experiments. Variable temperature experiments were performed by allowing the NMR tube to equilibrate in the magnet for five minutes after the desired temperature was reached.

Crystallography

Single colorless plate-shaped crystals of **1** and **2** were grown via slow evaporation of methanol and DMSO-d_6, respectively. For **1**, data was collected at Texas Christian University at 100 K on a Bruker D8Quest Diffractometer. Diffraction data for **2** was collected at Texas A&M University at 110 K on a Bruker Photon 3 kappa microsource diffractometer. Data collection, frame integration, and data reduction were carried out using APEX2 software.[44] Initial structure determinate and refinements were performed using XT structure solution program and refined by full matric least squares

Table 2. ^{1}H NMR spectroscopy allows the calculation of exchange rates (k_{exch}; sec^{-1}) at the coalescence temperature (T_c; K) as well as calculation of $\Delta G^{\ddagger}$ (kcal/mol).

		400 MHz				500 MHz	
#-Solv.	Res	k_{exch}	T_c	$\Delta G^{\ddagger}$	k_{exch}	T_c	$\Delta G^{\ddagger}$
	α	–	–	–	317	268	13.5
1-MeOD	B	–	–	–	–	–	–
	C	–	–	–	1644	281	13.3
	α	–	–	–	100	258	13.6
1-MeCN	B	–	–	–	–	–	–
	C	–	–	–	1157	273	13.1
	B	284	317	16.1	–	–	–
2-DMSO	C	228	315	16.0	–	–	–
	β-Me	–	–	–	–	–	–
	B	324	316	15.8	558	321	16.0
2-MeOH	C	105	308	16.2	121	309	16.3
	β-Me	46	296	16.1	106	304	16.1
	B	190	311	16.1	331	319	16.2
2-MeCN	C	746	321	15.8	887	333	16.3
	β-Me	92	304	16.3	168	309	16.1
	B	267	326	17.0			
2-D_2O	C	34	308	16.9			
	β-Me	58	316	17.1			
	B	755	336	16.5	329	341	16.7
2-Pyr.	C	214	321	16.6	277	329	16.8
	β-Me	–	–	–	–	–	–
	M1,2	261	350	18.0	–	–	–

[a] Decoalescence was not observed. The coalesced value is reported.

minimization using XL.[45,46] All non-hydrogen atoms were refined anisotropically while hydrogen atom positions were calculated geometrically and refined using the riding model.

Calculations of T_c and associated errors

T_c was calculated by plotting chemical shifts as a function of temperature. Three lines were fit for each resonance. Two were defined by the positions of the last two resonances prior to coalescence. A third was extrapolated back from coalesced resonances. The intersection point was used as the T_c whenever possible. Alternatively, the temperatures of the last decoalesced resonances and first coalesced resonances were averaged.

The errors reported in $\Delta G^{\ddagger}$ derive from uncertainty in estimates of Tc and δ. A 5 K range (±2.5 K) and δ ± 0.1 ppm were used to recalculate errors for $\Delta G^{\ddagger}$. These values rarely exceeded 0.1 kcal/mol. The choice of a 5 K range derives from the 5 K separation between data points, consistent with reported strategies.[31] The choice of a 0.2 ppm range derives from our evaluation of the data. The Supporting Information provides $\Delta G^{\ddagger}$ calculations of using these errors, underscoring the negligible differences that result.

Computation

Electronic structure calculations use the Gaussian 16 package.[47] Geometries in Figure 2 are obtained from conformational search with the CREST program. Computed geometries are included as Supporting Information. DFT calculations use the ωB97X-D exchange-correlation functional, the 6−31+G(d,p) basis set, the SMD continuum model for water solvent, and fully optimize the geometry. Chemical shifts are computed as isotropic chemical shieldings, computed with gauge-including atomic orbitals, relative to those computed for tetramethylsilane (TMS) at the same level of theory. NMR chemical shift calculations in Table 1 treat the doubly protonated macrocycle in model solvent with carbonyls pointed inward. The folded endpoints are identified as isoenergetic global minima in Figure 2, and are consistent with the folded structures observed experimentally in solution. The other local minima observed are consistent with motion along a proposed hinging coordinate that interconverts the isoenergetic global minima. The predicted energies of these local minima are high enough to have negligible contributions to the equilibrium NMR spectra, and low enough to be below the experimental interconversion barrier obtained from NMR coalescence temperatures. Overall, these results are consistent with the prediction that the observed NMR coalescence arise from 360° hinging motion of the macrocycle.

Conclusion

In summary, evidence for hinge motion derives primarily from variable temperature NMR spectroscopy which captures hinge motion between two closed states which are observed both crystallographically and in solution. DFT calculations support the model by identifying intermediates along a folding pathway and corroborating the observed chemical shifts.

The leaves of **1** and **2** sweep through 360° to adopt identical (enantiomeric) folded conformations observed in solution and solid-state studies. Motion is revealed by the coalescence of two or three different resonances in the ^{1}H NMR spectrum. The rate of hinge motion – from closed to open and back to closed – varies with steric congestion. Increasing steric hinderance on the backbone of the macrocycle by replacing a methylene with a geminal dimethyl group slows the rate of hinging. Hinge motion is largely independent of solvent choice based on agreement in $\Delta G^{\ddagger}$ values.

DFT calculations provide insight into the mechanistic basis for hinge motion and the origins of the difference in $\Delta G^{\ddagger}$ (3.0 kcal/mol) between **1** and **2**. This experimentally observed value is intuitively satisfying as it is similar in magnitude to values calculated for the rotational barrier calculated for amino-isobutyric acid residues appearing in peptides (4 kcal/mol)[54] and the barrier about geminal dimethyl groups in branched alkanes.[55]

We find the hinging behavior of these molecules both interesting and potentially useful. Through the lens of drug design, the ability of these molecules to dramatically alter their shape to bury hydrogen bonding groups translates into more favorable solubility properties (logP). Through the lens of material science, hinging from closed to open states dramatically changes the aspect ratio of the molecule which could manifest in interesting physical properties upon incorporation into a polymer.

Acknowledgements

We thank the NIH (R15GM 135900), the Robert A. Welch Foundation (P-0008), and the TCU SERC program for support.

Conflict of Interests

The authors declare no conflict of interest.

Data Availability Statement

The data that support the findings of this study are available in the supplementary material of this article.

Keywords: hinge · macrocycle · triazine · computation · variable temperature NMR

[1] Q. Chen, R. Menon, L. J. Calder, P. Tolar, P. B. Rosenthal, *Nat. Commun.* **2021**, *13*, 6314.
[2] J. C. Champoux, *Ann. Rev. Biochem.* **2001**, *70*, 369.
[3] R. D. Vale, R. A. Milligan, *Science* **2000**, *288*, 88.
[4] R. Muraoka, K. Kinbara, T. Aida, *Nature* **2006**, *440*, 512.
[5] X. Yang, Q. Cheng, V. Monnier, L. Charles, H. Karoui, O. Ouari, D. Gigmes, R. Wang, A. Kermagoret, D. Bardelang, *Angew. Chem. Int. Ed.* **2021**, *60*, 6617.
[6] M. N. Chatterjee, E. R. Kay, D. A. Leigh, *J. Am. Chem. Soc.* **2006**, *128*, 4058.
[7] G. Fioravanti, N. Haraszkiewicz, E. R. Kay, S. M. Mendoza, C. Bruno, M. Marcaccio, P. G. Wiering, F. Paolucci, P. Rudolf, A. M. Brouwer, D. A. Leigh, *J. Am. Chem. Soc.* **2008**, *130*, 2593–2601.
[8] E. Pazos, P. Novo, C. Peinador, A. E. Kaifer, M. D. García, *Angew. Chem. Int. Ed.* **2019**, *58*, 403.
[9] E. Uhl, P. Mayer, H. Dube, *Angew. Chem. Int. Ed.* **2020**, *59*, 5730.
[10] S. Kassem, T. van Leeuwen, A. S. Lubbe, M. R. Wilson, B. L. Feringa, D. A. Leigh, *Chem. Soc. Rev.* **2017**, *46*, 2592.

[11] N. N. Bach, V. Josef, H. Maid, H. Dube, *Angew. Chem. Int. Ed.* **2022**, *61*, e202201882.
[12] J. Echavarren, M. A. Y. Gall, A. Haertsch, D. A. Leigh, J. T. J. Spence, D. J. Tetlow, C. Tian, *Angew. Chem. Int. Ed.* **2021**, *143 (143)*, 5158.
[13] K. Grill, H. Dube, *Angew. Chem. Int. Ed.* **2020**, *142*, 19300.
[14] R. Hernandez, H.-R. Tseng, J. W. Wong, J. F. Stoddart, J. I. Zink, *J. Am. Chem. Soc.* **2004**, *126*, 3370.
[15] S. J. Chen, Y. Wang, T. Nie, C. Bao, C. Wang, T. Xu, Q. Lin, D.-H. Qu, X. Gong, Y. Yang, L. Zhu, H. Tian, *Angew. Chem. Int. Ed.* **2018**, *140*, 17992.
[16] C. Wang, S. Wang, H. Yang, Y. Xiang, X. Wang, C. Bao, L. Zhu, H. Tian, D.-H. Qu, *Angew. Chem. Int. Ed.* **2021**, *60*, 14836.
[17] Y. Gisbert, S. Abid, C. Kammerer, G. Rapenne, *Chem. Eur. J.* **2021**, *27*, 12019.
[18] S. Amano, S. D. P. Fielden, D. A. Leigh, *Nature* **2021**, *594*, 529.
[19] A. Sabatino, E. Penocchio, G. Ragazzon, A. Credi, D. Frezzato, *Angew. Chem. Int. Ed.* **2019**, *58*, 14341.
[20] C. D. Gutsche, L. J. Bauer, *J. Am. Chem. Soc.* **1985**, *107*, 6052.
[21] A. D. Hamilton, D. Van Engen, *J. Am. Chem. Soc.* **1987**, *109*, 5035.
[22] S. Shinkai, G. X. He, T. Matsuda, A. D. Hamilton, H. S. Rosenzweig, *Tetrahedron Lett.* **1989**, *30*, 5895.
[23] P. Dumy, M. Keller, D. E. Ryan, B. Rohwedder, T. Wolhr, M. Mutter, *J. Am. Chem. Soc.* **1997**, *119*, 918.
[24] H. J. Schneider, F. J. Werner, *Chem. Commun.* **1992**, *6*, 490.
[25] R. N. Warrener, D. N. Butler, L. Liu, D. Margetic, R. A. Russell, *Chem. Eur. J.* **2001**, *7*, 3406.
[26] J. Clayden, S. P. Fletcher, S. J. M. Rowbottom, M. Helliwell, *Org. Lett.* **2009**, *11*, 2313.
[27] S. Ernst, G. Haberhauer, *Chem. Eur. J.* **2008**, *73*, 2404.
[28] Y. Norikane, N. Tamaoki, *Org. Lett.* **2004**, *6*, 2595.
[29] C.-K. Koo, B. Lam, S.-K. Leung, M. H. W. Lam, W.-Y. Wong, *J. Am. Chem. Soc.* **2006**, *128*, 16434.
[30] C. Schouwey, M. Papmeyer, R. Scopelliti, K. A. Severin, *Dalton Trans.* **2015**, *44*, 2252.
[31] C. D. Jones, L. J. Kershaw Cook, D. Marquez-Gamez, K. V. Luzyanin, J. W. Steed, A. G. Slater, *J. Am. Chem. Soc.* **2021**, *143*, 7553.
[32] L. Feng, Y. Wang, K. Zhang, K.-Y. Wang, W. Fan, X. Wang, J. A. Powell, B. Guo, F. Dai, L. Zhang, R. Wang, D. Sun, H.-C. Zhou, *Angew. Chem. Int. Ed.* **2019**, *58*, 16682.
[33] G. W. Bemis, M. A. Murcko, *J. Med. Chem.* **1996**, *39*, 2887.
[34] S. Sankararaman, G. Venkataramana, B. Varghese, *J. Org. Chem.* **2008**, *73*, 2404.
[35] R. Nandya, S. Sankararaman, *Org. Biomolec. Chem.* **2010**, *8*, 2260.
[36] Y. Ai, M. H. Y. Chan, A. K. W. Chan, V. W. W. Yam, *Proc. Nat. Acad. Sci.* **2019**, *116*, 13856.
[37] A. J. Menke, N. C. Henderson, L. Kouretas, A. Estenson, B. G. Janesko, E. E. Simanek, *Molecules* **2023**, *28*, 1144.
[38] R. Capelli, A. J. Menke, H. Pan, B. G. Janesko, E. E. Simanek, G. M. Pavan, *ACS Omega* **2022**, *7*, 30291.
[39] V. R. Sharma, A. Mehmood, B. G. Janesko, E. E. Simanek, *RSC Adv.* **2020**, *10*, 3217.
[40] A. J. Menke, C. J. Gloor, L. E. Claton, M. A. Mekhail, H. Pan, M. D. Stewart, K. N. Green, G. M. Pavan, R. Capelli, E. E. Simanek, *J. Org. Chem.* **2023**, *88*, 2692.
[41] A. R. Katritzky, I. Ghiviriga, P. J. Steel, D. C. Oniciu, *J. Chem. Soc. Perk. Trans 2* **1996**, *3*, 443.
[42] H. E. Birkett, J. C. Cherryman, A. M. Chippendale, P. Hazendonk, R. K. Harris, *J. Molec. Struct.* **2002**, *602 (603)*, 59.
[43] D. Casarini, L. Lunazzi, A. Mazzanti, *Eur. J. Org. Chem.* **2010**, *11*, 2035.
[44] O. V. Dolomanov, L. J. Bourhis, R. J. Gildea, J. A. K. Howard, H. Puschmann, *J. Appl. Crystallogr.* **2009**, *42*, 339.
[45] G. M. Sheldrick, *Acta Cryst. Sect. C* **2015**, *71*, 3.
[46] G. M. Sheldrick, *Acta Cryst. Sect. a* **2015**, *71*, 3.
[47] Gaussian 16 Rev. C.01; Wallingford, CT, **2016**.

Manuscript received: March 29, 2023
Accepted manuscript online: May 25, 2023
Version of record online: July 7, 2023